metrologia

Performance of the PTB reconstructed primary clock CS1 and an estimate of its current uncertainty

A. Bauch, B. Fischer, T. Heindorff and R. Schröder

Abstract. The paper describes the current performance of the primary clock CS1 of the Physikalisch-Technische Bundesanstalt (PTB). The clock employs a thermal atomic beam and magnetic state selection. After major reconstruction during 1995 and 1996, routine clock operation was restarted in May 1997. Results of comparisons with UTC(PTB) and other internationally recognized time scales are presented. An evaluation of the CS1 Type B uncertainty yielded 7×10^{-15} ($1\ \sigma$). The CS1 is thus the most accurate atomic clock in continuous operation world-wide.

1. Introduction

The PTB primary clock CS1 has belonged to the group of so-called primary standards of frequency and time since 1969. Until 1978 it was operated intermittently and used for steering the PTB atomic time scales TA(PTB) and UTC(PTB). Between 1978 and 1995, the CS1 was operated continuously as a clock. It obtained maximum statistical weight in the ALGOS algorithm in use at the Bureau International de l'Heure (BIH), and since 1988 at the Bureau International des Poids et Mesures (BIPM), for the realization of the Free Atomic Time Scale, EAL (Échelle Atomique Libre). It was also one of the small number of clocks which allowed the difference between the scale unit of EAL and the SI second as realized on the rotating geoid to be determined with a specified uncertainty, thereby contributing to the realization of International Atomic Time, TAI (Temps Atomique International).

Inevitably, many components of the CS1 were subject to ageing. It was, therefore, decided to undertake major refurbishment, in the course of which all parts that had proved to be satisfactory were to be kept, while others for which improvements had been found were to be replaced. The vacuum system, in particular, had not been opened or modified since 1978 and required refurbishment. New getter-ion pumps were installed. At the same time, an improved microwave cavity was installed inside a newly-built central vacuum chamber. The quantization field was perfected. This work was carried out between summer 1995 and early 1996 and was followed by a test period during which the clock frequency and frequency instability were determined as functions of operational parameters such as beam current, microwave power, and C-field strength. The final action was the replacement of the caesium charge of the oven, which had been in place since 1982 and could have operated even beyond February 1997. Quasi-routine operation was restarted on 1 May 1997, since when clock data have been made available to the BIPM. Finally, it is found that this combination of measures has led to a considerably reduced uncertainty of the CS1 [1] compared with an estimate made some years ago [2]. As a result, the CS1 frequency should agree with the unperturbed hyperfine splitting frequency of ^{133}Cs, $f_0 = 9\ 192\ 631\ 770$ Hz, with an uncertainty of 7×10^{-15} ($1\ \sigma$).

This paper is organized as follows. A brief description of the CS1 is given below, followed by a description of the procedures adopted for operating it as a primary clock. Section 4 deals with the evaluation of the uncertainty. The CS1 has been compared with UTC(PTB) and with other internationally recognized time scales. Results have proved the excellent performance of the clock, as can be inferred from Section 5. We round off with some general conclusions.

2. Description of the CS1

2.1 General remarks

A primary clock is generally designed to ensure the best performance in terms of accuracy, frequency instability and reliability. There is no unique best solution in the design, because it is impossible to obtain optimal results simultaneously in all fields: compromises have to be made. In the case of the PTB primary clocks, high

A. Bauch, B. Fischer, T. Heindorff and R. Schröder: Time Unit Section, Physikalisch-Technische Bundesanstalt, Bundesallee 100, D-38116 Braunschweig, Germany.

accuracy has been a matter of greater concern than a low short-term frequency instability. At the same time, it was possible to operate the clocks continuously for many years so that they ensured the high quality of the PTB atomic time scales. The CS1 served as the model for all clocks subsequently developed at the PTB. The original design by Becker et al. [3] differed from that of clocks existing at that time because it comprised

(a) an axially symmetric atomic beam system, with magnetic lenses for the state selection, a point beam source, and a small detector on axis;

(b) an axial magnetic quantization field;

(c) a microwave cavity with smooth (sinusoidal) amplitude variation of the magnetic microwave field along the direction of the atoms' trajectories inside each irradiation section;

(d) slow square-wave frequency modulation for detecting the line centre.

Here, (a) is the most decisive feature because it allows the use of state-selecting magnets at the same time as efficient velocity filters, which select slow atoms in a narrow velocity range from a large solid angle. Accurate evaluation of most frequency-shifting effects is facilitated when the above design principles are combined.

Some details of the individual features are given below.

2.2 Atomic beam system

Figure 1 shows a schematic view of the CS1 vacuum system as it is now. The two end chambers house the oven and detector, respectively, including the associated pair of six-pole and four-pole magnets. The "magnetic lenses" in use in the CS1 have been in place since about 1976 and were designed according to considerations by Becker [4, 5]. The information given below is mainly taken from the technical drawings of that time and differs slightly from the data in [5].

Two tandem magnet systems are built into the CS1; each of these consists of a four-pole magnet facing the oven and detector, respectively, and a six-pole magnet facing the central vacuum chamber. The length of the four-pole magnet is 13.7 mm, and its pole tips are conically shaped. The distance between opposing tips increases from 1.6 mm to 2.45 mm. The maximum magnetic field strength at the pole tip is 700 kA/m and changes along the length of the bore [5]. The pole tips of the six-pole magnets have a total length of 9 mm; the distance between opposing pole tips is 3 mm, and the maximum magnetic field strength at the pole tips is 770 kA/m. A gap of 3.7 mm separates the two magnets. In the oven chamber, a beam stop, 0.8 mm in diameter, is mounted at the exit of the six-pole magnet. It blocks the direct line-of-sight between the nozzle of the oven and the detector. At the same time, it determines the width of the velocity interval of atoms reaching the detector.

The use of this type of magnet dictates to some extent the geometry of the oven nozzle and of the detector. The image of the atomic source, i.e. of the oven nozzle, is projected on to the entrance of the analyzer magnet with large magnification, given by the ratio of the distance between polarizer and analyzer and the focal length of the magnet. Thus the useful nozzle diameter is limited to below 0.1 mm [4]. It is actually 0.1 mm, and the nozzle has a channel length of 0.5 mm. The analyzer focuses atoms to a spot less than 1 mm in diameter and located in the focal plane, a few millimetres behind the exit of the four-pole magnet. The active element of the detector, a 1 mm^2 Pt-Ir filament, is situated here and held at +7 V potential. The evaporated caesium ions are deflected towards a collector at ground potential. A repeller at +7 V prevents ions from migrating to other grounded metal surfaces, thus ensuring maximum efficiency of the detector. To obtain a sufficiently strong beam flux, the temperature of the oven is maintained at 170 °C. Using standard equations and tabulated data for the caesium vapour pressure [6], a total beam flux from the oven of 5.6×10^{13} atom/s is estimated. The 5 g caesium charge

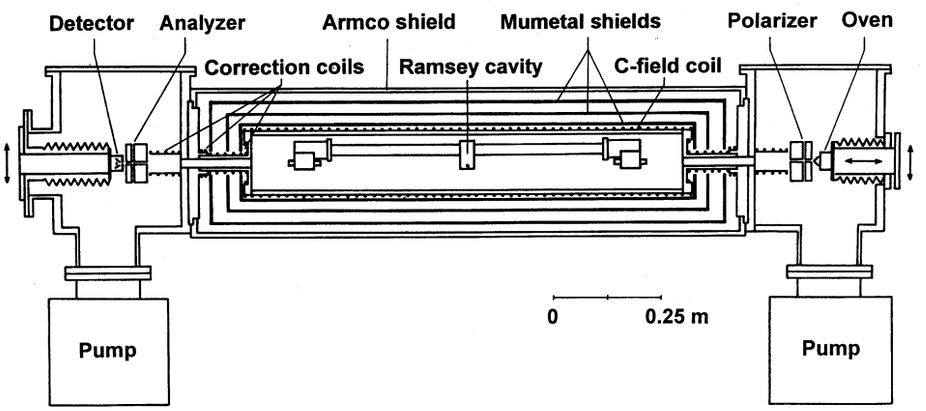

Figure 1. Vertical section through the reconstructed CS1 primary clock.

of the oven should thus allow continuous operation until the year 2010.

During the recent refurbishment the atomic beam generating system was kept as it had been before, except that the detector was rebuilt. Thus the velocity distributions of the atoms in the Zeeman substates have remained almost unchanged [5]. The spectrum of the ($\Delta F = 1$, $\Delta m_F = 0$) microwave σ-transitions is shown in Figure 2. The resonance transitions are observed in a flop-out configuration: that is, atoms having made a microwave transition are deflected from the detector. A high-resolution record of the different lines enables the determination of the relative populations and the velocity distributions of the atoms in the m_F states. It turns out that less than 10 % of the atoms in the beam are in the "clock state", ($F = 4$, $m_F = 0$). Figure 3 shows the velocity distributions of atoms in the states ($F = 4$, m_F), $m_F = 0, \pm 1$. The mean velocity of atoms in the clock state is 94.7 m/s and the velocity distribution has a relative full width at half maximum of 8.5 % (see Section 4.2 for the underlying numerical procedure). The large population asymmetry is a consequence of magnetic state selection and implies that a rather high strength of the quantization field is used. Thus a large separation in frequency between individual lines in Figure 2 has to be chosen in order to minimize Ramsey and Rabi pulling (see Sections 4.3.2 and 4.3.3).

2.3 Quantization field (C-field)

The magnetic shield consists of three layers of Mumetal, 5 mm in thickness, and an outer soft-iron case of 10 mm thickness. Many years ago, the axial and transversal shielding factors were determined to be 3×10^4 and greater than 10^6 [7], respectively. More recently, the axial shielding factor of the CS2 magnetic shield, of essentially the same dimensions, was also found to be greater than 2×10^4. The quantization field, usually named the C-field, is generated by a solenoid, wound on to the aluminium vacuum chamber, and correction coils at each end. Throughout this paper, the term "field" is used for the magnetic flux density expressed in teslas. A single current supply unit is used for all coils, but only certain fractions of the current pass through the individual correction coils. In this way the region of excellent homogeneity has been extended to cover the full length of the microwave cavity. Figure 4 shows a plot of the residual field and the C-field inside the CS1; these data were recorded after the final field adjustment during clock assembly. The mean C-field strength is 8.27 μT, and the relative inhomogeneity of the C-field within the region of the microwave cavity is 2.7×10^{-4} (rms). Two additional pairs of coils, located at both sides of the vacuum flanges which separate the end chambers and the main chamber of the CS1, are used to generate a guiding field outside the Mumetal shields, in continuation of the C-field up to the state-selecting magnets. Adiabatic atomic transport is thereby ensured (see Section 4.3.1).

2.4 Microwave cavity

One of the most critical parts of a caesium atomic clock is the microwave cavity, because several requirements have to be met:

(a) In order to minimize pulling effects, the resonance frequency of the cavity should coincide with f_0. Its sensitivity to temperature variations which occur inside the clock during operation should not degrade clock performance (see Section 4.4.2 on cavity pulling and 4.4.1 on phase difference).

(b) The phase difference between the two interaction regions of the cavity should be stable, and the

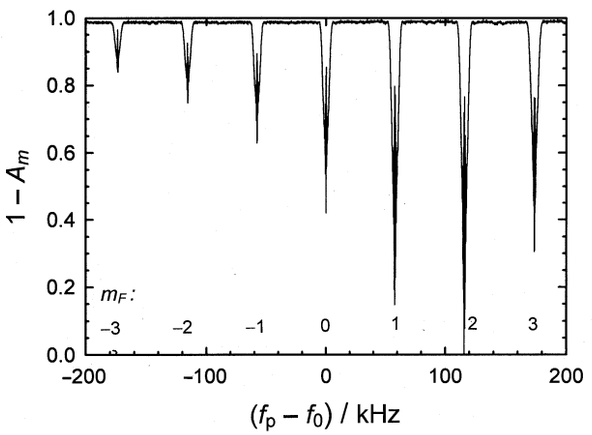

Figure 2. Microwave resonance signals recorded in the CS1 with fixed microwave magnetic field amplitude which yielded the maximum amplitude A_0. A_m is the normalized resonance amplitude of the $(4, m_F)$–$(3, m_F)$ transition; $f_p - f_0$ is the frequency detuning of the microwave probing frequency from the (4,0)–(3,0) resonance frequency f_0.

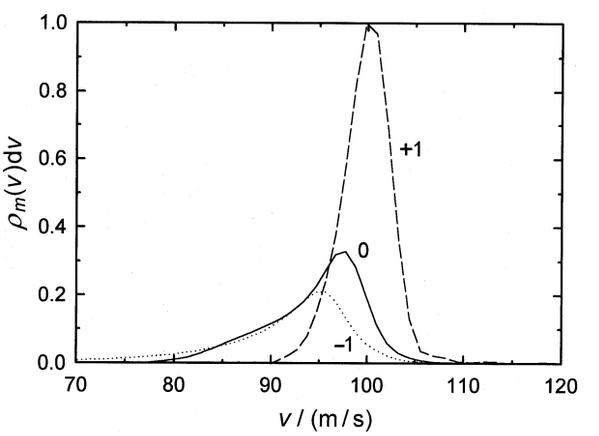

Figure 3. Velocity distributions $\rho_m(v)\mathrm{d}v$ of atoms in the Zeeman states $(4, m_F)$, $m_F = 0, \pm 1$ (marked next to the curves). The area under the curves reflects the relative population of the states.

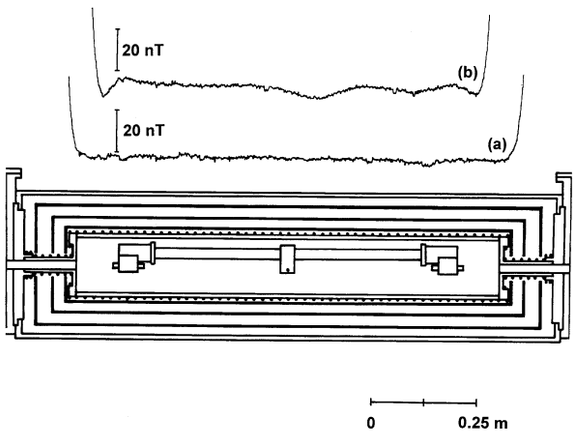

Figure 4. Plots of the axial magnetic field in the beam tube of the CS1. The position of the cavity, the magnetic shields, the solenoid and the correction coils are shown for clarity; (a) residual ambient field, C-field current off; (b) C-field after final adjustment of the current through the correction coils. In both cases, the origin of the ordinate has been shifted by different amounts.

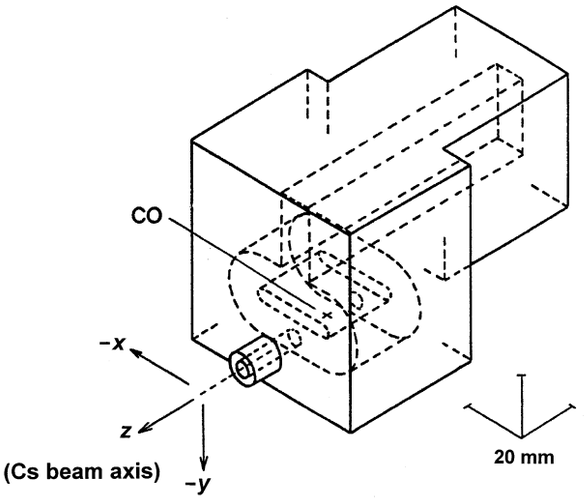

Figure 5. End section of the CS1 microwave cavity. CO is the midpoint of the irradiation section and origin of the coordinate axes. The end sections have been machined from OFHC copper and the parts have been soldered together; dimensions are given in the text.

phase gradients perpendicular to the atomic beam inside the irradiation sections should be known by experiment or theory and should be small.

(c) The mechanical and electrical design of the cavity, including its feed, should prevent microwave field leaks.

There is no doubt that the old CS1 cavity was imperfect with regard to these requirements, and recognition of this stimulated the decision to rebuild the clock. In contrast to the previous design of the CS1, the microwave cavity as a whole is now installed in the new central vacuum chamber. The cavity consists of the central waveguide, 28 half-wavelengths in length ($28\ \lambda_g/2 = 651.5$ mm, where λ_g is the wavelength corresponding to f_0 in a standard X-band waveguide), which is similar to the cavity used in other PTB clocks such as the CS3 [8] and the CSX [9]. Two terminal parts of ring-shaped design, as proposed by De Marchi et al. [10], are attached. Their length in the z-direction, as explained in Figure 5 (63.4 mm), is slightly in excess of $2.5\ \lambda_g/2$ and has been adjusted so that the joint with the central part coincides with a plane of zero longitudinal surface currents in the waveguide. The two interaction regions of length $\ell = 23.3$ mm are thus separated by the drift length $L = 731.7$ mm.

The three parts of the cavity are joined by titanium screws, and all joints are equipped with soft metallic gaskets which efficiently suppress leakage of microwave fields through the slits. Cut-off tubes, 5 mm in diameter and 22.5 mm in length, reduce microwave leakage through the beam holes. An analysis of the modes inside the cut-off tubes yields a damping of 200 dB with respect to the field strength at the centre of the irradiation sections [8]. Measurements of the field as a function of distance into the tubes, made using a miniaturized loop antenna inside the tubes and a highly sensitive spectrum analyzer, supported this value.

Figure 5 is a diagram of one end section. The main purpose of the ring structure is to sustain a microwave field with a maximum magnetic field and a zero Poynting vector at CO, the midpoint of the irradiation section and the origin of the coordinate axes in Figure 5. The ring is strongly coupled to the straight part of the cavity. The dimensions of the ring have been chosen such that the coupling resonance is centred at about 9.2 GHz (full width at half maximum, about 200 MHz) and that four half-wavelengths fit into the ring. An unwanted high-Q resonance, which may lead to a shift of the symmetry point in the ring, is excited if there are small asymmetries between the two arms of the ring. Its resonance frequency is 9.5 GHz, clearly different from the normal working frequency. The mechanical dimensions of the end sections now in use differ slightly from those of the units studied previously [11]. More recently [12], it was pointed out that, in view of the dependence of the end-to-end phase difference on cavity dimensions, it would have been even more advantageous to choose the dimensions such that the coupling of the ring is anti-resonant.

Close to the beam axis, the microwave magnetic field component B_z, parallel to the C-field, is described by

$$B_z(z) = B_0 \cos(\pi x/d) \cos(\pi z/\ell). \qquad (1)$$

Here, B_0 is the maximum of the microwave magnetic field which is parallel to the z-axis in CO, ℓ is the length of the irradiation section ($\ell = 23.3$ mm), and d is one-quarter of the ring circumference ($d = 22.2$ mm). The transverse magnetic microwave field B_x which is responsible for the excitation of the (extremely weak) $\Delta F = 1$, $\Delta m_F = \pm 1$, π-transitions, is given by

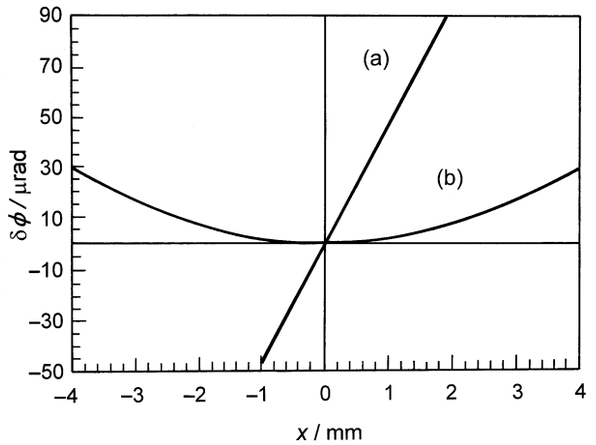

Figure 6. Predicted spatial phase variation for standard X-band copper waveguide in two different configurations: (a) atomic beam passing at a distance of λ/2 from the waveguide short and (b) beam passing at the phase minimum in a ring cavity (reproduced from [10]).

$$B_x(z) = -B_0\,(d/\ell)\sin(\pi x/d)\sin(\pi z/\ell). \qquad (2)$$

Thus $B_x(z)$ depends almost linearly on the distance x of the trajectories of the atoms from the symmetry line, $x=0$, whereas $B_z(z)$ is practically independent of x. The line shape of the σ-transitions ($\Delta F=1$, $\Delta m_F=0$) agrees well with a field shape described by (1), whereas the line shape of the π-transitions ($\Delta F=1$, $\Delta m_F=\pm 1$) is slightly distorted, probably [13] as a result of beam holes in the cavity (see Figure 13).

The spatial variation of the phase of the microwave field around CO in the x-direction is predicted to be quadratic [10], as can be inferred from Figure 6. For comparison, the figure includes the linear phase gradient prevailing in a corner-shaped end section of a standard X-band copper waveguide, as employed in the CS2 and CS3 clocks of the PTB (see for example [8]). The ring-shaped cavities thus appear very promising. An experimental investigation of these cavities did not show full agreement with the predictions and this is discussed in detail in Section 4.4.1, in which the determination of the end-to-end phase difference of the CS1 is outlined.

The resonance frequency of the cavity was tuned to agree with f_0 in vacuum at a temperature of 297 K with an uncertainty of 1 MHz. Because the value of the loaded Q is low, at 450, typical temperature variations do not cause detuning, which would entail significant cavity pulling or power shift, as detailed below.

2.5 Electronics

In the CS1, a commercial 5 MHz BVA voltage-controlled quartz oscillator (VCXO) is slaved by means of the control loop to yield an output frequency in accordance with the definition of the second. The control loop in Figure 7 shows the following elements: VCXO, frequency-synthesis unit, caesium-beam tube and signal-processing unit. The design criteria have been laid down in [14]. In the frequency-synthesis unit the signal of the VCXO at $f_n = 5$ MHz is converted to the signal in the microwave region at frequency f_p. It is

$$f_p = 1840\ f_n - f_s = f_0 + f_e, \qquad (3)$$

with $f_e = 2.918\ 592$ Hz and $f_0 = 9\ 192\ 631\ 770$ Hz.

In closed-loop operation, f_p is steered to the actual line centre of the clock transition, which differs from f_0 by the sum of all systematic frequency shifts. This implies that f_e is approximately equal to the frequency shift due to the quadratic Zeeman effect (by far the largest of the systematic effects), which in turn is dictated by the C-field of about 8.27 μT. The adjustment of the C-field strength is explained in the following section. Ultimately, the value of f_s and thus that of f_e is determined by the frequency-synthesis electronics [14]. The numerical value for f_e in (3) is strictly valid only in the long-term average and assuming zero uncertainty. To determine the line centre, the frequency f_p is square-wave modulated with a modulation period T_m of 260 ms. The total time constant of the control loop is about 30 T_m. The modulation width can be set to $f_H = 62$ Hz, which corresponds to the width W of the central Ramsey fringe, or $f_H = 186$ Hz (3 W). When the modulation width f_H is changed, some systematic frequency shifts may emerge, as explained in Section 3. More details of the electronics are given in Section 4.5.

To summarize this section, Table 1 specifies the operational parameters of the CS1.

Table 1. Operational parameters of the CS1.

Oven temperature	170 °C
Cs charge and its lifetime	5 g; 13 a
Mean atomic velocity	94.7 m/s
Width of velocity distribution	8.2 m/s
Interaction length ℓ of cavity	2.327 cm
Separation L between interaction regions	73.2 cm
Linewidth of clock transition	63.2 Hz
Mean C-field strength	8.27 μT
Frequency instability $\sigma_y(\tau)$	$5\times10^{-12}\ (\tau/\mathrm{s})^{-1/2}$

3. Operation of the CS1

As in the past, the CS1 is operated as a primary clock. The quartz oscillator in the CS1 control loop is the physical source of the 1 pps signal T(CS1) and of 5 MHz signals used for frequency comparisons. The time difference $[UTC(PTB) - T(CS1)]$ was arbitrarily set to 20 000 ns on 1 May 1997, Modified Julian Day (MJD) = 50569. It is impossible to guarantee the uncertainty stated below without repeated control of the experimental parameters of the clock. Therefore the C-field strength is determined from a measurement of the Zeeman frequency (see Section 4.1.1) and

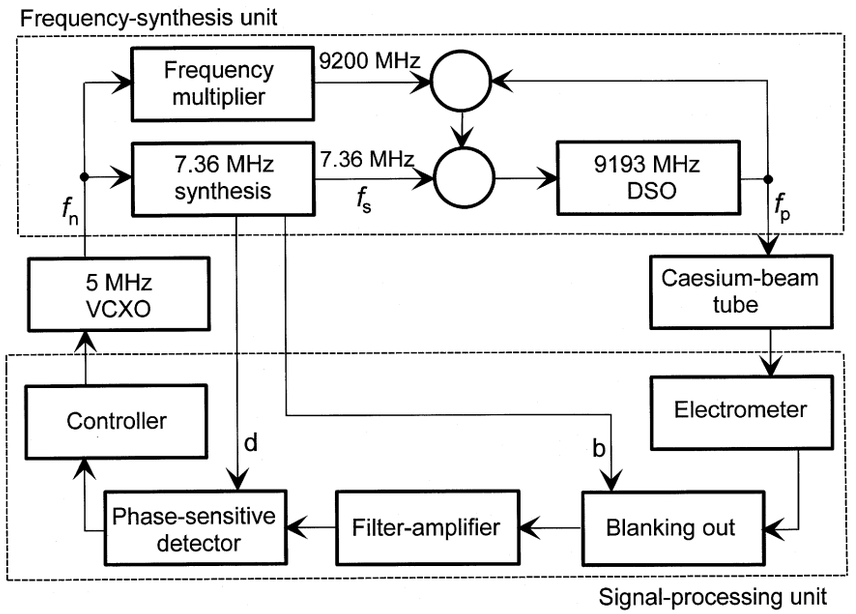

Figure 7. Electronic system used to lock the frequency of the 5 MHz voltage-controlled quartz oscillator (VCXO) to the atomic resonance in the CS1; DSO is the dielectrically stabilized oscillator.

the microwave power level is determined from the response of the atoms at resonance, $f_\mathrm{p} \approx f_0 + f_\mathrm{e}$, with a Type A uncertainty of about 0.3 dB. Both quantities are manually set to the appropriate level. A linewidth measurement gives the mean velocity, and the correction for the quadratic Doppler effect is applied according to the measurement result (see Section 4.2). Such "normal" servicing is typically carried out twice per week, as can be inferred from Figure 8 (101 points in 360 days). The spectral purity of the microwave signal and a few signals in the electronics are recorded in order to monitor the correct functioning of the equipment, usually on the occasion of a beam reversal event, about once every eight weeks (see Figure 15). In this case, the two end chambers are interchanged in position. This can be accomplished without breaking the vacuum in the three main sections of the apparatus, but clock operation has to be interrupted for about 6 hours. Of course, the control loop has to be opened during all service work. In order to avoid a loss of coherence in the 5 MHz signal and a time step in T(CS1), the quartz oscillator is phase-locked during the servicing work to an external 5 MHz signal from one of the PTB atomic clocks whose frequency differs from that of CS1 by less than 2×10^{-14}. The accumulated time error in this slaved mode thus is about 100 ps during the one-hour period required for "normal" servicing work. If the interruption lasts longer, such as after a beam reversal, the time difference $[UTC(PTB) - T(CS1)]$ is reset to the predicted value with a precision of 100 ps.

After each beam reversal, the C-field strength has to be readjusted. As explained above, the sum of the corrections due to the quadratic Zeeman effect, the quadratic Doppler effect, cavity phase difference,

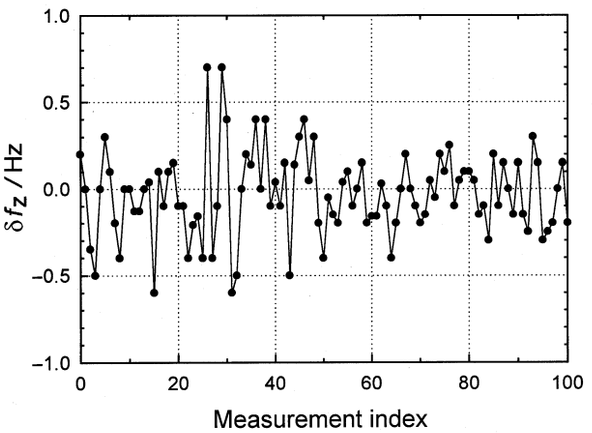

Figure 8. Measured deviation δf_Z between actual and nominal value of the Zeeman frequency f_Z as a function of time. Measurements were taken once every 2 to 4 days from MJD 50569 to MJD 50925. A deviation δf_Z of 1 Hz would indicate that in the preceding time interval the clock frequency was in error by 1×10^{-14}.

and gravity, has to be made equal to $-f_\mathrm{e}/f_0$ (3). In particular, as the frequency shift due to the cavity phase difference is opposite in sign in the two beam directions, the C-field strength has to be changed by about 0.1 % after each beam reversal.

A dependence of the clock frequency on f_H would be present in case of a sloped baseline on which the Ramsey fringes are superimposed. This would occur if the cavity is coarsely detuned from f_0 or if the C-field strength is much smaller than its nominal value. When spurious microwave fields are present in the beam tube one might also expect a dependence of the clock frequency on f_H, in particular when they

are combined with non-optimum microwave excitation (see Section 4.3.1). Therefore $f_H = 3\ W$ was frequently used during the first operation of the modernized CS1, until May 1997, and occasionally thereafter.

Based on knowledge of the velocity distribution and the end-to-end phase difference, and assuming only minor cavity detuning from f_0, one can predict the frequency dependence on microwave power for both beam directions and both values of f_H. At a microwave power level 3 dB above optimum, the maximum predicted frequency shift is -3×10^{-15}. At this power level, the CS1 frequency instability is increased by a factor of 1.6, still sufficient for reliable operation of the clock electronics. Microwave power variations have thus been introduced and results have shown a deviation by up to a factor of two from the predictions (see Section 4.3.1), even after all detectable microwave leaks had been removed. Nevertheless, these data have been included in the total sample presented in Section 5.

4. Frequency corrections F_i and estimation of their uncertainties δF_i

The evaluation of the CS1 uncertainty has mainly been carried out along the lines previously published for the CS3 [8]. Treatment has to a certain extent been influenced by De Marchi's paper [15], and for exhaustive theoretical explanations the reader is referred to [6]. The frequency corrections and their uncertainties have been compiled in Table 2 and are dealt with in some detail below.

4.1 Frequency shifts related to external fields

4.1.1 Magnetic field: quadratic Zeeman effect

The presence of the C-field B_C in the interaction region increases the clock transition frequency by $f_C = 0.0427$ Hz $(B_C/\mu T)^2$. The determination of the relative frequency correction, $F_C = -f_C/f_0$, comprises measurements of the mean C-field strength, its inhomogeneity and its temporal instability. Before clock operation was started the relative inhomogeneity was inferred to be 2.7×10^{-4} (rms) from plots of the axial field component as shown in Figure 4. Later, the central Ramsey fringes were centred on top of the Rabi pedestals of the magnetic-field-dependent microwave transitions by adjusting the currents through the correction windings at the ends of the C-field coil. Thereafter, the field averaged over the two irradiation sections differs from the mean field in the drift region by less than 3×10^{-6}, relatively. The total Type B uncertainty of F_C is, at most, 1×10^{-15}.

Table 2. CS1 frequency corrections and their uncertainties.

Cause of frequency shift	$10^{15} \times$ Relative correction	$10^{15} \times$ Relative uncertainty
Quadratic Zeeman effect	–317 500	1
Stark effect (thermal radiation)	17	0.5
Quadratic Doppler effect	50	0.5
Majorana transitions	0	2
Ramsey pulling	0	3
Asymmetry of microwave spectrum	0	0.2
Cavity phase difference	310	6
Cavity detuning	0	0.3
Electronics	0	1

A Type A contribution to the uncertainty was determined by repeated determinations of F_C. It is common practice to determine F_C from a measurement of the Zeeman frequency f_Z, i.e. the separation between the (4,1)-(3,1) and the (4,0)-(3,0) transitions. The following is valid:

$$F_C = -8\,(f_Z/f_0)^2\,(1 + f_Z/f_0)$$
$$\text{and} \quad \delta F_C \approx -16\, f_Z\, \delta f_Z / f_0^2, \tag{4}$$

where δf_Z represents a small variation of f_Z. In Figure 8 the results of f_Z measurements are plotted as a time series, the 101 measurements being fairly equally distributed within the time interval MJD 50569 to MJD 50925. A histogram plot of the result (Figure 9) confirms that the individual measurements are normally distributed around a mean of –0.03 Hz. The standard deviation of 0.24 Hz (relative value $\approx 4 \times 10^{-6}$), thus corresponds to a Type A uncertainty of 3×10^{-15} during time intervals between checks of the magnetic field. This contribution should, however, average to zero with time and is therefore not included in Table 2.

4.1.2 Electric fields: Stark effect

Static electric fields inside a grounded and highly-conductive metal enclosure are generally considered to be so small that no significant frequency shift due to the dc Stark effect should occur [6]. The electric fields of thermal radiation emitted from the surface of the enclosure are, however, known to produce a significant frequency shift due to the ac Stark effect, f_{acS} [16]. The theoretical predictions were verified experimentally with a 10 % accuracy in 1996 [17], more recent measurements of the dc and ac Stark effects allow f_{acS} to be estimated with an uncertainty which is principally limited by the uncertainty of the temperature measurement and of the spectrum of the prevailing radiation [18]. According to [17, 18], the clock transition frequency is shifted by

$$f_{acS} = -1.573\,(3) \times 10^{-4}\,\text{Hz} \times (T/300\,\text{K})^4 \times$$
$$[1 + 0.0014\,(T/300\,\text{K})^2] \tag{5}$$

in the presence of thermal radiation from a perfect black body at temperature T.

The inner structure of the CS1 can be seen in Figures 1 and 4. Three Pt-100 thermoresistors

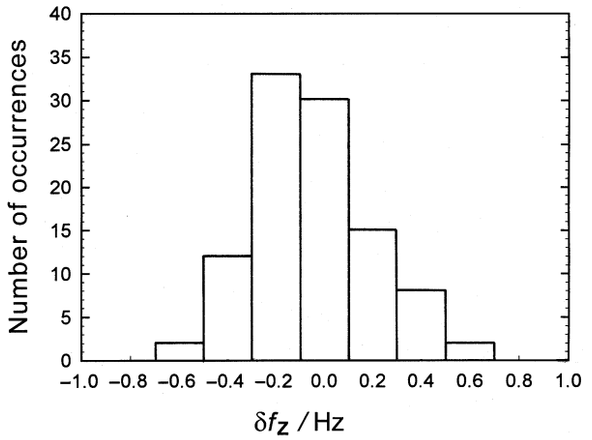

Figure 9. Measured deviation δf_Z between actual and nominal value of the Zeeman frequency f_Z, plotted as a histogram. Measurements were taken once every 2 to 4 days from MJD 50569 to MJD 50925. A normal distribution apparently describes the data quite well.

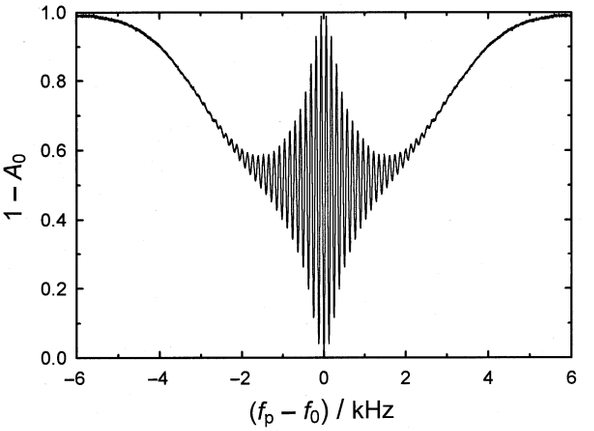

Figure 10. Ramsey pattern of the clock transition as recorded in the CS1. A_0 is the normalized resonance amplitude; $f_p - f_0$ is the frequency detuning of the microwave probing frequency from the (4,0)–(3,0) resonance frequency f_0.

have been attached to the outside of the C-field support cylinder whose inner surface determines the intensity and spectrum of the thermal radiation. The temperature is thus known to be 297.0 K, with a Type B uncertainty of 0.5 K, estimated from the specifications of the thermoresistors and the apparent temperature distribution along the C-field support. The surfaces in the oven and detector end chambers are at a temperature somewhat higher than that of the main chamber. Geometric considerations have led to the conclusion that the radiation field is that of a nearly perfect black body at 297.0(5) K, with a relative standard uncertainty in the emissivity of 2 %. The correction $F_{\mathrm{acS}} = -f_{\mathrm{acS}}/f_0$ is thus 16.7×10^{-15} with a Type B uncertainty of 0.5×10^{-15}. Continuous monitoring of the mean temperature in the CS1 revealed variations of less than 0.5 K peak-to peak over the last 10 months, except for a few days in mid-August 1997, when temperature control in the clock hall failed. Thus, the Type A uncertainty is negligible. The correction F_{acS} is included in Table 2, but is not routinely applied either to the CS1 clock data or to the CS2 and CS3 clock data. Thereby a frequency step has been avoided in the PTB Free Atomic Time Scale TA(PTB), which has been directly derived from the primary clocks for two decades.

4.1.3 Gravitational fields

General relativity predicts a relative increase in the frequency of a clock operated above the rotating geoid, of 1.09×10^{-16} m^{-1} [19]. The CS1 is designed to contribute to the formation of TAI. TAI is a *coordinate* time scale, with the SI second, as realized on the rotating geoid, as its scale unit. A relative frequency correction F_{G} of -8.7×10^{-15} is thus applied to the CS1 frequency, allowing for the 79.5 m height of the CS1 atomic beam above the geoid. As the height can easily be inferred from nearby geodetic reference points whose common reference is the Amsterdam zero sea level, the uncertainty of F_{G} is of the order of 10^{-16}. As an academic aside, it should be mentioned that the correction F_{G} is not significant for the realization of the *proper* second and thus need not be included in the total uncertainty budget of the clock.

4.2 Time dilation: relativistic Doppler effect

Special relativity predicts that due to time dilation the clock frequency observed in the laboratory frame is shifted by

$$f_{\mathrm{D}} \approx [-v^2/(2c)^2] \times f_0 \qquad (6)$$

compared with the eigenfrequency in the rest frame of the atoms, f_0, when the atoms move with velocity v in the clock. It is known that the recorded Ramsey pattern of the clock transition, which is shown in Figure 10, contains the information necessary for estimating v and thus f_{D}. The simplest approach makes use of the fact that in the case of optimum excitation, i.e. when the (fictive) atomic spin [6] is rotated by $\pi/2$ in each irradiation section of the cavity, the mean velocity $\langle v \rangle$ of atoms contributing to the resonance signal is related to the linewidth W of the central Ramsey fringe by

$$\langle v \rangle = 2\, L_{\mathrm{C}}\, W, \qquad (7)$$

where L_{C} is the effective drift length of the cavity ($L_{\mathrm{C}} = L + 1.204\ \ell$), for a monokinetic beam [20]. In the case of the CS1, $W = 62.92$ Hz, $L_{\mathrm{C}} = 0.760$ m, thus $\langle v \rangle$, as defined by (7), is 95.6 m/s. By inserting $\langle v \rangle$ in (6), $F_{\mathrm{D}} = -f_{\mathrm{D}}/f_0$ is found to be 51×10^{-15}. Because the width of the velocity distribution is less than 0.1 $\langle v \rangle$, the mean squared velocity $\langle v^2 \rangle$ [to be inserted in (6)] and $\langle v \rangle^2$ from (7) differ by only about 1 %, and any

detailed calculation of the velocity distribution $\rho(v)\mathrm{d}v$ and of F_D will thus result in F_D being equal to the above value to within one or two parts in 10^{15}. For completeness, the essentials of the numerical treatment of the Ramsey pattern are repeated from a previous paper [21].

In a first step it is assumed that the central portion of the Ramsey pattern is described by

$$P_2 = \frac{1}{2}\int_0^\infty \rho(T')\,\{1\}\,[1+\cos(\Omega_0 T')]\,\mathrm{d}T', \tag{8}$$

where $\rho(T)\mathrm{d}T$ is the distribution of times of flight through the section of length L_c, and $\Omega_0 = 2\pi\,(f_\mathrm{p} - f_0)$. The numerical factor $\{1\}$ replaces $\sin^2(2b\tau)$, where b is the Rabi frequency as defined in [22] and τ is the time of flight through one irradiation section. This so-called optimum excitation, $\sin^2(2b\tau) = 1$, which gives the maximum amplitude of the central Ramsey fringe, can be established with an uncertainty of about 0.3 dB. From a cosine transform of (8), $\rho(T)$ is obtained and converted to $\rho(v)$. In an iterative step, $\rho(v)$ is divided by $\sin^2[\langle v\rangle/(v\pi/2)]$ to obtain a new distribution which turns out to be only marginally wider than $\rho(v)$. Here $\langle v\rangle$ denotes the velocity average over $\rho(v)$. In Figure 11 the final distribution $\rho_0(v)\mathrm{d}v$ for the atoms in state (4,0), and the difference between the two iterations, $\delta\rho_0(v)\mathrm{d}v$, are illustrated. The above replacement has obviously been essentially correct for all contributing velocities. $\rho_1(v)\mathrm{d}v$ and $\rho_{-1}(v)\mathrm{d}v$ are shown in Figure 3. $\rho(v)$ is used to calculate the transition probability P_1 as a function of $f_\mathrm{p} - f_0$. As the analytical relation for P_1 (e.g. equation 5.2.35 in [6]) does not apply to the case of a sinusoidal variation of the magnetic microwave field along the atoms' trajectories in the irradiation sections, a discretization procedure is applied. The amplitude $b(z)$, equal to $b(z) = \pi\ \mu_\mathrm{B}\ B_\mathrm{z}(z)/h$ for the clock transition, is decomposed into p segments, each of constant amplitude. Here, μ_B is the Bohr magneton and h the Planck constant. For each of the segments the analytical solution can be written as a 3×3 matrix. The full solution for one velocity then is the product of $p+1+p$ matrices, the middle one for the drift region. $p = 40$ is sufficiently exact. Summation over the (typically 110) velocity intervals allows the line shape of the σ-transition to be calculated; this method can be adapted also to the π-transitions. The same procedures can be used to calculate frequency shifts from $P_1\,(f_\mathrm{p} - f_0 = f_\mathrm{H}/2)$, $P_1\,(-f_\mathrm{H}/2)$, and the slope $\mathrm{d}P_1\,(f_\mathrm{H}/2)/\mathrm{d}f_\mathrm{p}$. The second-order Doppler effect, phase differences, cavity detuning and spatially variable atomic resonance frequency can be modelled in the calculations. In addition, the influence of microwave power and of a sloped baseline, and the dependence of the apparent line centre on the modulation width f_H, can be checked. Examples of these calculations are mentioned below in Section 4.3.

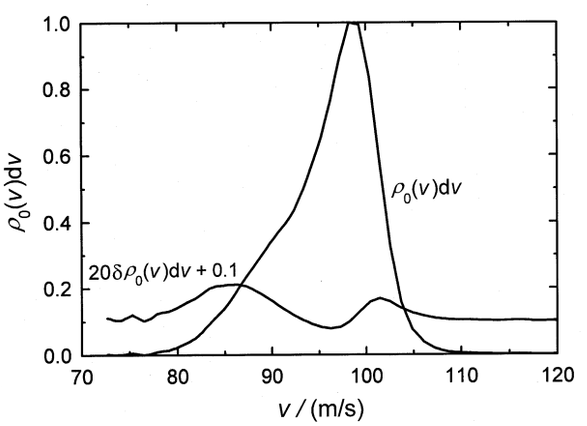

Figure 11. Velocity distribution $\rho_0(v)\mathrm{d}v$, obtained iteratively as explained in the text by correcting for the term $\sin^2(2b\tau)$ which was replaced by 1 in (7), and plot of $20\,[\delta\rho_0\,(v)\,\mathrm{d}v]$, shifted upwards by 0.1.

Here, we concentrate on the second-order Doppler effect. F_D is calculated to be 49.8×10^{-15} with a Type B uncertainty of 0.5×10^{-15}. The estimated uncertainty includes variations of the microwave power during recording of the Ramsey patterns and variation of the noise in the input data by variation of the signal integration time per frequency step. The reader may compare the final value of F_D with the results of the first approach made at the beginning of this section. The situation would be much less advantageous if the velocity distribution were equal or close to the modified Maxwell-Boltzmann distribution, as is the case when state preparation is performed by optical pumping. Much more effort has been found to be indispensable in this case to determine b while recording the Ramsey pattern and to obtain an acceptably low uncertainty in F_D [23, 24]. An analysis of the methods applied in [23, 24] revealed that they are less suitable in the case of a narrow velocity distribution and would not reduce the above uncertainty in the determination of F_D.

One problem is to determine the correct value of L_c in the case of a velocity distribution of finite width [20]. The smallest deviation between recorded and calculated Ramsey patterns was obtained with $L_\mathrm{c} = L + 1.196\ \ell$. The first side lobe of the clock transition Ramsey pattern, corresponding to $\Omega_0 T = \pi$ in (8) ($P_2 = 0$, maximum beam signal), has a frequency separation W' from the line centre, $\Omega_0 T = 0$, which is almost equal to W. During clock operation, servicing includes a measurement of W' again using slow square-wave frequency modulation around $f_\mathrm{p} - f_0 = W'$, as W' is a good measurement quantity and more easily accessible than W itself. However, W' is sensitive to the modulation width f_H chosen in the measurement, as follows from experiment and calculations. Figure 12 proves that the experimental results nicely follow the theoretical prediction. On the one hand, this again gives confidence in the corrections of the numerical

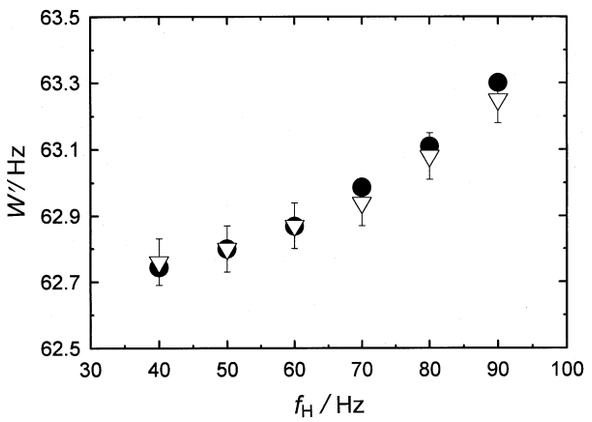

Figure 12. Frequency separation W' of the centre of the first side lobe of the clock transition Ramsey pattern from f_0 as a function of the modulation width f_H. ▽, measurement results with measurement uncertainty; ●, calculation, based on $\rho_0(v)\mathrm{d}v$ from Figure 11.

treatment outlined above. On the other hand, one can find the required relation between F_D and W': $F_D = 1.3 \times 10^{-17} \times (W'/\mathrm{Hz})^2$ is valid at $f_H = 62$ Hz. W' has not changed by more than 0.2 Hz throughout routine operation of the CS1. It can be affected significantly by deliberate modifications of the beam optics, such as the distance between the oven nozzle or the detector filament, respectively, and the nearby magnetic lens. Changes in W' have not been found to be correlated with beam reversals.

4.3 Frequency shifts related to the multilevel structure of ^{133}Cs

The ^{133}Cs atom has sixteen ground-state sublevels with quantum numbers $F = 4$, $m_F = -4, \cdots, +4$ and $F = 3$, $m_F = -3, \cdots, +3$. Typically, the clock transition is considered as being excited in an isolated two-level system, but no perfect isolation is possible. Three kinds of couplings among the various sublevels may lead to frequency shifts of the clock transition.

(a) Inhomogeneous static magnetic fields along the beam path between polarizer and analyzer may induce Majorana transitions ($\Delta F = 0$, $\Delta m_F \neq 0$).

(b) Microwave magnetic field components transversal to the quantization field are unavoidable because of the transverse extension of the atomic beam and the field mode in the cavity [see (2)]. The frequency shift which may result is known as Ramsey pulling [25].

In both cases, an atom leaving the polarizer magnet in a certain initial state (4, m_F) can reach its final state in which it is detected along various paths in the quantum space [26]. As the paths are indiscernible, the transition amplitudes interfere, affecting the clock transition Ramsey pattern.

(c) Easier to explain is frequency pulling due to the asymmetry of the neighbouring σ-transition lines, shown in Figure 2. Even if a frequency close to f_0 is fed to the cavity there is a non-zero probability that the neighbouring σ-transitions are excited. The corresponding frequency shifts have been designated Rabi pulling [27].

4.3.1 Majorana transitions

Frequency shifts due to Majorana transitions will occur if all the following prerequisites are met [26]:

(a) The transport of the state-selected atoms between polarizer and analyzer magnet is non-adiabatic.

(b) With respect to total number and velocity, the population of Zeeman sublevels in the atomic beam is a function of the quantum number m_F.

(c) $\Delta F = \pm 1$, $\Delta m_F = \pm 1$ transitions are induced in the microwave interaction region by microwave magnetic field components transverse to the longitudinal C-field.

In the CS1, the last two prerequisites are unavoidably fulfilled. The condition of adiabatic transport can be expressed by the dimensionless parameter $\exp[-\pi^2\, \mu_B\, B^2/(4\, v\, h\, \mathrm{d}B_z/\mathrm{d}z)]$, which must be close to zero everywhere along the path of the atomic beam. Here, B is the local magnetic field strength and $\mathrm{d}B_z/\mathrm{d}z$ is the derivative taken at the same point. In the cavity region, $B^2/(\mathrm{d}B_z/\mathrm{d}z)$ is sufficiently large that adiabatic transport prevails. In addition, between the state-selecting magnets and the microwave cavity, guiding magnetic fields are produced with the various coils seen in Figure 4. They prevent B from approaching zero.

In the CS1, the adiabatic transport condition was verified in so far as it was confirmed that the velocity distributions of the atoms in the states (4, m_F) are not affected by moderate field changes around the normal strength. On the other hand, no theory is known which would allow a *quantitative* estimate of potential frequency shifts in the presence of Majorana transitions. Therefore the uncertainty estimate has to rely on the results of frequency measurements made under a range of conditions. In [26] it is shown that the influence of Majorana transitions can also be demonstrated effectively by changing the microwave power. These kinds of experiment have been undertaken because small changes of the guiding fields did not produce any significant frequency shift. At the same time, however, it is known that spurious microwave irradiation along the beam path between polarizer and analyzer can also entail large and time-varying frequency shifts and, in particular, lead to an increased sensitivity of the clock frequency to microwave power [8, 28]. It is thus not easy to distinguish from a single type of experiment whether any observed power dependence originates from Majorana transitions or microwave

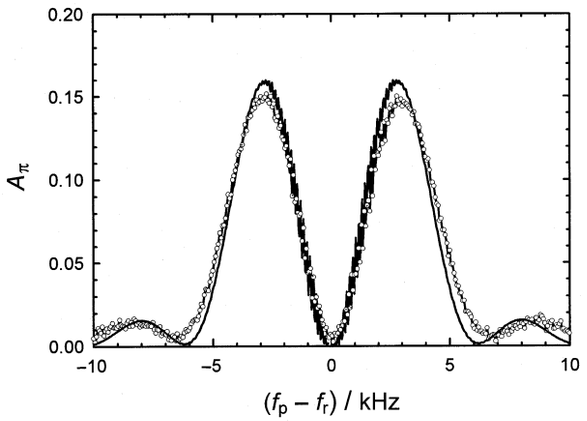

Figure 13. Line shape of the $(F = 4, m_F = 1)$–$(F = 3, m_F = 0)$ and $(F = 4, m_F = 0)$–$(F = 3, m_F = 1)$ π-transition at a microwave power 15.8 dB above the optimum for the clock transition; solid line denotes calculation with parameters as given in the text, open circles denote experimental curve; the resonance amplitude A_π is given normalized to A_0 from Figure 10; $f_p - f_r$ is the frequency detuning of the microwave probing frequency from the centre frequency of the resonance, f_r, which is about $f_0 + f_Z/2$.

leakage. During several time intervals between June 1996 and May 1998 the CS1 was operated at microwave power levels up to 3 dB above the optimum value. No relative shifts exceeding 2×10^{-15}/dB around optimum power were measured. The uncertainty contribution of 2×10^{-15} has been included in Table 2 under the heading "Majorana transitions", but this may not be an appropriate description.

4.3.2 Ramsey pulling

$\Delta F = \pm 1$, $\Delta m_F = \pm 1$ π-transitions do occur, even if Figure 2 suggests otherwise. Increase of the microwave power by 15.8 dB above the optimum value allowed the transitions to be recorded with a good signal-to-noise ratio. In Figure 13, the $(F = 4, m_F = 1)$–$(F = 3, m_F = 0)$ and $(F = 4, m_F = 0)$–$(F = 3, m_F = 1)$ transitions, both approximately at the same resonance frequency, are shown. The experimental curve is compared with a calculation in which microwave power level, population of the Zeeman levels, the field shape (2) and the 3 mm beam diameter were taken as input parameters. The slight difference between the widths of both curves can be explained qualitatively by distortions of the field mode due to the presence of the beam hole in the cavity [13].

The presence of this type of unwanted excitation of the atoms may lead to a frequency shift, that of Ramsey pulling, which was first calculated by Cutler et al. [25] for short commercial frequency standards in the case of a misalignment between the directions of the C-field and the microwave magnetic field, this latter being assumed to be constant in amplitude. Ramsey pulling turned out to constitute a shift of the resonance frequency, which oscillates with C-field value and decreases as the C-field strength increases. In [25], time-independent perturbation theory was used to derive the population of the Zeeman levels behind the second irradiation section of the cavity. Interference terms, which contained mixed products of the initial probability amplitude of the population of different energy states, were removed on the basis of physically plausible arguments. The application of the final expression for the Ramsey pulling required knowledge of the velocity distributions of atoms contributing to the σ- and π-transitions on the high- and low-frequency sides of the clock transition.

In the CS1, transversal and longitudinal magnetic microwave fields in the irradiation section have a position-dependent amplitude. As an approximation to the field pattern of (1) and (2), each irradiation section had to be subdivided into a sufficient number of intervals, each of them with constant transversal and longitudinal amplitude. As a consequence, the interference terms could no longer be removed from the expression for the transition probability, but had to be removed from the final result by other methods. Normally, the CS1 is operated at a C-field strength of 8.27 μT. As a result of our calculations, Ramsey pulling should then be zero with a Type B uncertainty of 3×10^{-15}. In contrast, one may infer from Figure 4b in [25] a few parts in 10^{13} for Ramsey pulling in a short frequency standard. Details and final results will be reported elsewhere.

4.3.3 Asymmetry of the microwave spectrum

Because of the strong asymmetry of the CS1 microwave spectrum (see Figure 2), the clock is operated at a fairly high C-field strength and thus at a Zeeman frequency of about nine times the width of the Rabi pedestals. Favourably, the wings of the Rabi pedestals are strongly damped because of the sinusoidal variation of the microwave amplitude in the irradiation sections. In the far-off resonance approximation (equation 5.2.88 in [6]) they are described by

$$P_3 = \frac{15}{2}\pi^2 \{b_c \tau \cos(\Omega_R \tau/2)/[(\Omega_R \tau)^2 - \pi^2]\}^2, \quad (9)$$

where b_c is the maximum value of $b(z)$ in the irradiation section and $\Omega_R = 2\pi(f_p - f_0 \pm f_Z)$, with the minus sign for the (4,1)–(3,1) transition and the plus sign for the (4,–1)–(3,–1) transition. P_3 is calculated as an average over $\rho_1(v)$ and $\rho_{-1}(v)$, respectively, shown in Figure 3, and is added to P_1. The frequency shift f_{RI}, resulting from the sloped baseline underlying P_1, is calculated as explained in Section 4.2. As Figure 14 shows, Rabi pulling at the Zeeman frequency as used in the CS1 is well below 2 parts in 10^{16}. The sensitivity of this shift to microwave power variations around the working point would be less than 2×10^{-16}/dB and thus is insignificant.

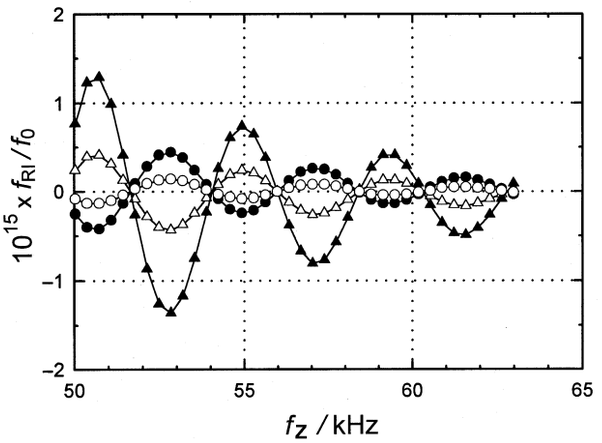

Figure 14. Calculated relative frequency shift f_{RI}/f_0 of the clock transition in the CS1 as a result of pulling by the neighbouring transitions. The velocity distributions shown in Figure 3 were used as input data. Results are given for optimum microwave power (open symbols) and increased microwave power (+3 dB, filled symbols) and two modulation widths $f_{\mathrm{H}} \approx W$ (circles) and $f_{\mathrm{H}} \approx 3\ W$ (triangles). The connecting lines serve as visual aids only.

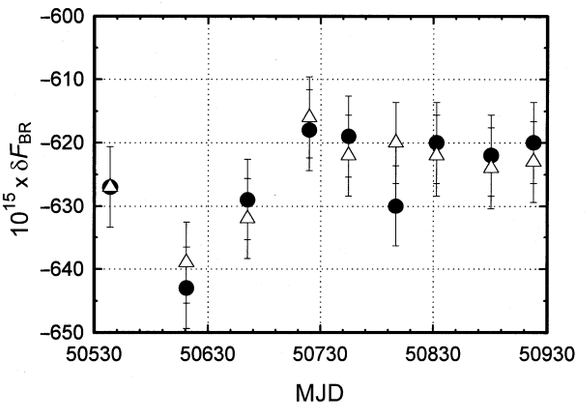

Figure 15. Relative CS1 beam reversal frequency shift δF_{BR}, determined since April 1997. Each data point is the difference of frequency averages over 12 to 18 days before and after the date of the beam reversal, expressed by its Modified Julian Day (MJD). MJD 50930 = 27 April 1998; ●, weighted average of measurements related to the group of the PTB atomic clocks; △, mean of measurements related to UTC(NIST), UTC(USNO) and UTC(SU). The error bars reflect the statistical uncertainty (1 σ) predicted from shot-noise and thermal noise of the CS1 alone.

4.4 Frequency shifts related to the microwave cavity

4.4.1 End-to-end cavity phase difference

In all atomic clocks using Ramsey's separated oscillatory field method, the existence of a phase difference ϕ between one end and the other of the microwave cavity proves to be one of the main impediments to achieving an uncertainty in the low 10^{-15} range. The phase difference ϕ is governed by the differences of the electrical lengths of the two cavity arms and the differences in the reflection properties of the two end sections of the cavity. The differences may stem both from geometrical imperfections and conductivity variations in the cavity material. It is thus obvious that ϕ will change whenever, for example, the length of one cavity arm changes with respect to the other. Recently it was shown that, under certain circumstances, the total length of the cavity may also influence ϕ [9, 12]. The frequency shift accompanying ϕ amounts to

$$f_\phi = -\phi v/(2\pi L), \tag{10}$$

and ϕ is interpreted as the phase in the irradiation section at the detector side of the cavity minus the phase at the oven side of the cavity. Thus f_ϕ can be determined either by variation of the atomic velocity v, as was applied in the CS1 many years ago [3], or by reversing the direction of the atomic beam. The latter method is now employed in the CS1, and for this purpose the positions of the two end chambers are interchanged. The CS1 frequency in both beam directions was measured with reference to the group of atomic clocks at the PTB – in most cases the CS2, three commercial caesium clocks, two active and one passive hydrogen masers – and also with reference to UTC(NIST), UTC(USNO) and UTC(SU) using standard GPS common-view comparisons.* The relative frequency differences between the two beam directions, δF_{BR} (BR for beam reversal), obtained since April 1997, are plotted in Figure 15. The last six results in particular agree perfectly within the error bars.

The difference δF_{BR} obtained in this way is naively identified as twice the relative frequency shift due to ϕ, and $\delta F_{\mathrm{BR}}/2$ is routinely applied with the appropriate sign as a frequency correction, as explained in Section 3. A value of $\delta F_{\mathrm{BR}} = -620 \times 10^{-15}$ would correspond to a phase difference of approximately 140 μrad. Of course, the frequency instability of the CS1 and of the reference clocks determines the precision of individual measurements of δF_{BR}. But as long as the clock is operated with alternate beam directions for equal periods of time θ, the mean clock frequency over a total interval $2k\ \theta$ (where k is a sufficiently large integer) becomes independent of ϕ with a negligible Type A uncertainty. This statement, however, is true only if ϕ and v in (10) have the same absolute value in both beam directions. While this is well fulfilled for v, it is not necessarily the case for ϕ.

One reason for this is the spatial variation of the phase of the microwave field in the interaction region, even if the use of ring cavities minimizes this effect. The spatial dependence of the phase in the x-direction around the phase minimum of a ring cavity (see Figure 5) is quadratic, and according to Figure 6 it

* NIST: National Institute of Standards and Technology, USA; USNO: United States Naval Observatory, USA; UTC(SU) is maintained by the Institute of Metrology for Time and Space (IMVP NPO VNIIFTRI), Russian Federation.

should remain within 4 μrad over the 3 mm diameter of the atomic beam [10]. Measurements at the PTB yielded less optimistic results, but they may have been corrupted by frequency shifts caused by microwave leakage, possibly present in the experimental apparatus that was used [11]. A worst-case estimate of those results is taken as the basis for the current uncertainty estimate, however, where we assume that the phase variations might be as large as 20 μrad/mm, much more than one would conclude from Figure 6 for a ring cavity, but still less than the 94 μrad/mm for the cavities employed in the CS2 and CS3 [29].

The spatial phase variations only have consequences if the atomic beam takes different paths in the two beam directions. In this case, ϕ for beam direction 1 is not equal to $-\phi$ in beam direction 2. Thus the beam retrace capability has to be determined. Despite the rather simple method of performing the beam reversal, it can be verified that the positions of the atomic beam in the two directions in any case lie in an interval 0.6 mm in width around the geometrical axis which is defined by the centres of the cut-off tubes of the cavity end sections. Assuming a square probability distribution, the corresponding standard deviation describing the beam retrace capability is $0.3\ \text{mm}/\sqrt{3} = 0.17$ mm, and a first Type B uncertainty contribution of 4×10^{-15} is estimated for the determination of $F_\phi = -f_\phi/f_0$.

Even if the beam retrace were perfect, $|\phi|$ could systematically be different in the two beam directions, simply because the cavity arm facing the oven becomes slightly warmer than the opposite arm. This problem is particularly significant for the CS1, whereas it practically does not exist in the case of the CS2 and the CS3: in these clocks ovens are mounted at both ends, and all ovens are kept warm all the time, irrespective of the beam direction.

As explained in Section 4.1.2, the temperature distribution along the central vacuum chamber which houses the cavity is continuously monitored by three Pt-100 resistors. Until MJD 50700, the end-to-end temperature difference changed by about 0.28 K when the oven position was changed. By additional heating, a reduction of the temperature difference to below 0.02 K was achieved. As one can infer from Figure 15, apparently δF_{BR} is slightly higher and less unstable after that epoch. In order to estimate the potential frequency-shifting effect, the sensitivity of ϕ of the CS1 cavity to temperature and temperature difference would need to be known. Experimental evidence has proved that these effects are substantial in a cavity which is similar, but not equal to, that in the CS1 [11]. To apply the results, the temperature of the cavity itself, not of its surroundings, would be needed. On the assumption that the temperature difference along the cavity could unaccountably and systematically vary by 0.1 K after each beam reversal, and combining this with the published temperature sensitivity, a second, independent Type B uncertainty contribution to F_ϕ of 3.5×10^{-15} has been taken into account. The combined value is given in Table 2.

4.4.2 Cavity detuning

The microwave magnetic field amplitude becomes different for the two probing frequencies $f_{\text{p}} = f_0 \pm f_{\text{H}}/2$ when the cavity resonance frequency deviates from f_0. As long as cavity detuning is limited to below 5 MHz, the resulting relative frequency shift is of the order of only 10^{-16} when the clock is operated at optimum excitation, simply because the transition probability P_2 becomes insensitive to b around optimum excitation, $b\ \tau = \pi/4$, (8). Of course, a shift is unavoidable at other microwave power settings. Given the parameters of the cavity as described in Section 2.4, detuning the cavity by 5 MHz would lead to a power shift coefficient of 4×10^{-15}/dB at $f_{\text{H}} = W$. Such a detuning could easily be detected by measuring the centre frequency of the clock-transition Rabi pedestal, which is more sensitive in this respect [30]. Detuning by 5 MHz would show up as a frequency offset of the Rabi pedestal by 0.28 Hz with respect to the essentially unshifted Ramsey fringe. It takes several hours of measurement to determine the line centre of the broad Rabi pedestal with the required accuracy. All measurements performed hitherto have given a zero shift of the Rabi pedestal with a measurement uncertainty of 0.05 Hz to 0.1 Hz, consistent with the frequency tuning of the cavity before it was mounted inside the clock. As long as the operating temperature of the CS1 remains stable, occasional routine checks allow the Type B uncertainty of the cavity pulling frequency shift to be estimated at 0.3×10^{-15}, as listed in Table 2.

4.5 Frequency shifts related to the electronics

Much has been said about physical effects which may shift the atomic transition frequency from its defined value f_0. All these effects play a role inside the caesium beam tube as shown in Figure 7. The remainder of this section deals briefly with the two functional parts of the electronics: the frequency-synthesis unit and the signal-processing unit. This is a summary of a previous analysis [8, 14] of the electronic system, seven copies of which have been built so far, in use with the PTB clocks and for some time with the Jet de Pompage Optique (JPO), of the Laboratoire Primaire du Temps et des Fréquences (LPTF), Paris.

The output microwave signal at frequency f_{n} contains spurious spectral components which have their origin in an improper blocking of the line frequency (and multiples thereof). In the case of perfectly symmetrical sidebands – i.e. no mixture of amplitude and phase modulation – no frequency shift occurs [31]. Sidebands at frequency multiples of 50 Hz are at least 60 dB below the carrier and symmetrical to better than 1 dB. Thus no systematic frequency shift larger than 5×10^{-16} is expected.

The output signal is generated by nonlinear processes from the input signal at frequency f_n. It thus cannot be a pure sine wave, but must contain phase modulation sidebands at multiples of the common subharmonic frequencies of f_p and f_n. All signals used for triggering the frequency modulation, the detection time window, labelled b in Figure 7, and the phase-sensitive detection, labelled d in Figure 7, originate from the VCXO and thus have a fixed phase relation to the synthesized frequency. By choosing a proper time window for the signal processing, the effect of these phase modulation sidebands can be completely suppressed [14].

In processing the signal coming from the beam tube, the transients occurring after switching f_p are suppressed during the blanking interval T_b and the signal is processed only during the time window T_a. The blanking serves two purposes. It allows a high gain of the filter amplifier to be used which would otherwise become saturated. What is more important, due to the nonlinear processes in the frequency synthesis, the transient response generally differs slightly for the two directions of frequency switching. This leads to a false determination of the line centre. The duration of T_b is dictated by these considerations: if T_b is greater than 25 ms, the potential frequency shift is less than 10^{-15}. But the choice of the ratio $T_b/(T_m/2) = 1/4$ and of $T_m = 16/62$ s is dictated by the requirement that the effect of the phase modulation sidebands must be suppressed, as mentioned above.

The control voltage which is fed to the VCXO is generated in an analogue circuit which contains a proportional and an integral path and subsequent signal filtering (PIT_1). So the linear frequency drift of the free-running VCXO, specified to be about 10^{-10}/day, is eliminated without an offset voltage at the input of the integrator, a signal which would result in a false determination of the line centre.

Offset voltages of a few microvolts might possibly occur in the phase-sensitive detector and the integrator, resulting in a false control voltage. To resolve this problem it is advantageous to choose the highest possible gain of the filter-amplifier (see above). Signal processing in the phase-sensitive detector and transients in the electrometer output at frequencies $1/T_m$ and $1/(2T_m)$ caused by the blanking interval have been studied in some detail. During operation of the CS1, the offset voltages are controlled several times per year. Based on previous experience, this ensures that the relative frequency shift originating from these never exceeds 1×10^{-15}.

5. Results

The performance of the rebuilt CS1 with respect to stability and accuracy is documented in this section based on measurements made during a period of almost one year. Comparisons of the CS1 with reference clocks within the PTB (Section 5.1) and with international time scales (Section 5.2) have yielded very promising results.

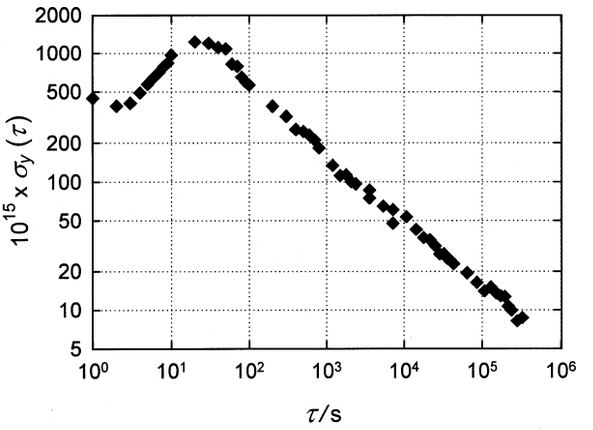

Figure 16. Relative frequency instability of the CS1 determined from comparisons with an active hydrogen maser (KVARZ CH1-75). The instability of the maser and that of the measurement system are negligible for all averaging times τ. The non-overlapping square root of the Allan variance $\sigma_y(\tau)$ is plotted. Error bars due to the finite number of samples are at most twice the size of the plotted symbols.

5.1 Internal comparisons

The short-term frequency instability of the CS1 has been evaluated several times in comparison with one of the PTB's active hydrogen masers (KVARZ, CH1-75). 5 MHz signals have been compared in a KVARZ phase comparator, a procedure which allows the CS1 frequency instability to be determined for all averaging times τ without contributing significant measurement noise. Typical data compiled in a $\sigma_y(\tau)$ diagram are shown in Figure 16. For averaging intervals a few times longer than the attack time of the CS1 control loop (about 10 s), $\sigma_y(\tau)$ follows perfectly the behaviour $\sigma_y(\tau) = 5 \times 10^{-12}/\sqrt{(\tau/\mathrm{s})}$ predicted from the CS1 atomic line Q, the clock transition signal (see Figure 2), shot noise and thermal-detector noise. The instability could be reduced only at the price of an intolerably large caesium consumption.

The long-term performance has been evaluated on the basis of comparisons with the PTB's currently working primary clocks CS2 and CS3. In Figure 17 the time residuals of the one-year comparison are shown. The apparent rate change around MJD 50630 seems to be a feature common to the CS2 and the CS3, which is not observed in comparisons of the CS1 against international scales. To obtain quantitative estimates, daily mean frequency differences were computed. To give an example, the combined frequency instability of CS1 and CS2 is 6×10^{-15} at $\tau = 10$ d and agrees with the shot-noise-limited performance of both clocks. For longer averaging times, $\sigma_y(\tau)$ remains almost constant, which must be attributed to instabilities, mostly of the

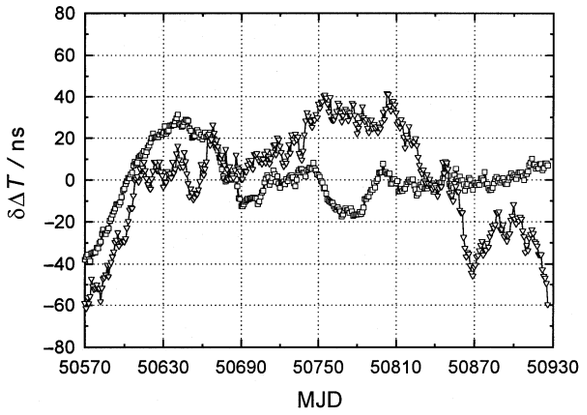

Figure 17. Results of time comparisons: $\Delta T = [T(CS3) - T(CS1)]$ (▽) and $\Delta T = [T(CS2) - T(CS1)]$ (□), illustrated by the time residuals $\delta\Delta T = \Delta T -$ linear trend.

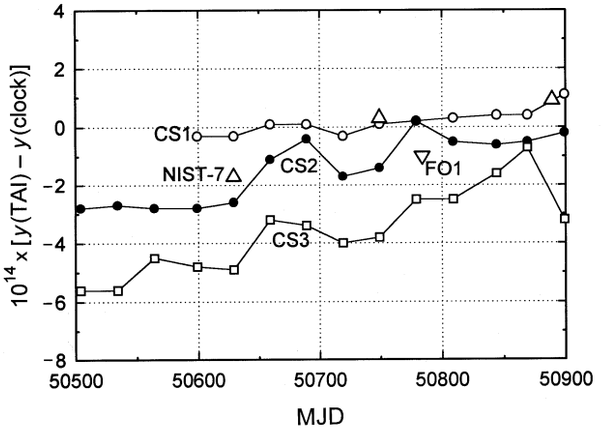

Figure 18. Frequency comparison of the primary clocks CS1 (○), CS2 (●), CS3 (□) of the PTB, NIST-7 (△) and FO1 (▽), with the international time scale TAI. The CS1 data were generated by adding the offset between CS1 and CS2 to the CS2 data, which were, like the other data, taken from the Annual Report of the BIPM Time Section, 1997, and from *Circular T*, 1998 (up to and including issue T123). The NIST-7 and FO1 data are averages over isolated time intervals of 5 or 10 days, whereas the PTB data are averages over contiguous 30-day intervals; the symbols are plotted at the end of the averaging interval. All clock data have been consistently corrected for the frequency shift arising from black-body radiation.

CS2, during the period under study. The CS3 appears to be more noisy.

The most striking fact is the one-year relative frequency difference, $y(\mathrm{CS3}) - y(\mathrm{CS1}) = 32 \times 10^{-15}$, exceeding the sum of the stated uncertainties, 7×10^{-15} for the CS1, and 14×10^{-15} for the CS3 [8]. The result $y(\mathrm{CS2}) - y(\mathrm{CS1}) = 12 \times 10^{-15}$, obtained during the same period, is more favourable and is within the CS2 uncertainty of 15×10^{-15} [2]. This difference has the same sign and is of the same order of magnitude as observed for almost a decade between 1986 and 1995, before the refurbishment of the CS1, which is remarkable after all the modifications to the CS1.

5.2 International comparisons

It seemed obvious to merge CS1 data with data from published comparisons of the TAI rate with primary clocks, although the CS1 was not contributing to the determination of the scale unit of TAI during the period under study. The results are plotted in Figure 18. One can clearly identify the frequency differences between the continuously operated primary clocks of the PTB, as well as their different behaviour. The CS1 data show the smoothest behaviour. The small upward trend seems to reproduce the steering of TAI. The accumulated frequency steering which has been applied to EAL, with the intention of bringing the TAI scale interval into agreement with the SI second, amounted to about 10^{-14} in relative units during the period under study. Steering was effected in predicted small steps of 1×10^{-15} to 2×10^{-15}, which are hidden in the noise of TAI and T(CS1). The steering had become necessary consequent to Recommendation S2 of the 13th Meeting of the Consultative Committee for Time and Frequency, stating that the second as realized with primary clocks is to be corrected for the ac Stark frequency shift due to the electric fields of thermal background radiation. The second is thus now shorter by about 1.7×10^{-14} s than it was a couple of years ago.

In Figure 18, a larger slope is inferred from the comparisons with CS2 and CS3, and it is difficult to decide which clock is most accurate. Data from other primary standards have been included in the figure. The NIST-7 uncertainty was specified as 7×10^{-15} for MJD 50624 and 1×10^{-14} for the other two data points, whereas the FO1 uncertainty was specified to be 3×10^{-15} [32]. For most of the time, agreement among the primary clocks is within their combined uncertainty, except for the CS3 which is systematically offset. The amount of data from NIST-7 and from the FO1 is rather limited, however, and does not really allow meaningful conclusions to be drawn.

Therefore, as a next step, a comparison of the CS1 against the free atomic time scales has been made. Obviously, such an analysis cannot answer the question regarding the accuracy of the primary clocks, but it allows the long-term frequency instability of the CS1 to be estimated. The comparisons are calculated from data $[TA(PTB)–T(CS1)]$, obtained at the PTB, and $[TAI - TA(k)]$, $k =$ NIST, USNO, SU and PTB, taken from the BIPM publication *Circular T*. This choice of time scales was motivated by the assumption that these time scales should be mutually independent and should be the most stable references continuously available today (see, for example, [33]).

Indeed, many more details about the behaviour of the CS1 can be inferred from the time residuals which are illustrated in Figures 19 and 20. When

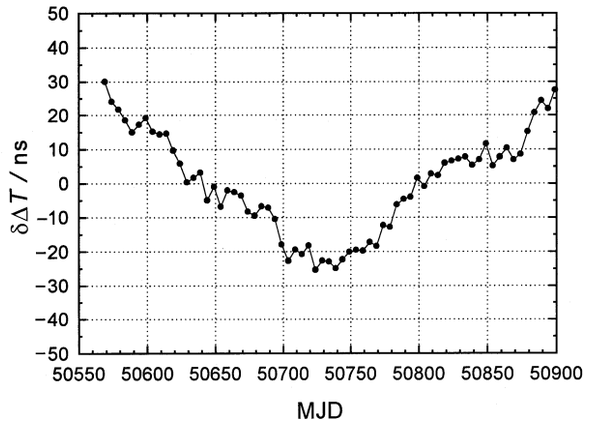

Figure 19. Results of time comparisons: $[\Delta T = TAI - T(CS1)]$ (●), illustrated by the time residuals $\delta\Delta T = \Delta T -$ linear trend.

TAI is compared with T(CS1), the time residuals show the signature of an increasing frequency difference, as expected from the preceding discussion on Figure 18. The slope here is about –0.5 ns/d at the beginning of the plot and +0.5 ns/d at the end.

The results shown in Figure 20 need more detailed consideration. The overall impression is that only small rate changes occurred between T(CS1) and TA(NIST) and TA(USNO), respectively. One may identify slope changes around MJD 50700 and around MJD 50820. The first epoch coincides with the beginning of the temperature regulation of the CS1 microwave cavity, which was explained in Section 4.4.1. A small CS1 frequency change could indeed be expected after that measure. At MJD 50820 a new value for the correction δF_{BR} was calculated and later applied. Because of the small number of beam reversals having been made until then, and the limited precision with which δF_{BR} can be determined from a single beam reversal event (see Figure 15), a small change in rate, detected only after the event, may be unavoidable. Such instabilities

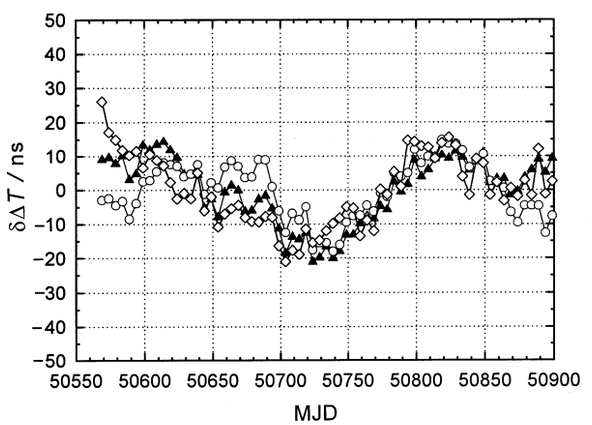

Figure 20. Results of time comparisons: $\Delta T = [TA(NIST) - T(CS1)]$ (▲), $\Delta T = [TA(SU) - T(CS1)]$ (◇), and $\Delta T = [TA(USNO) - T(CS1)]$ (○), illustrated by the time residuals $\delta\Delta T = \Delta T -$ linear trend.

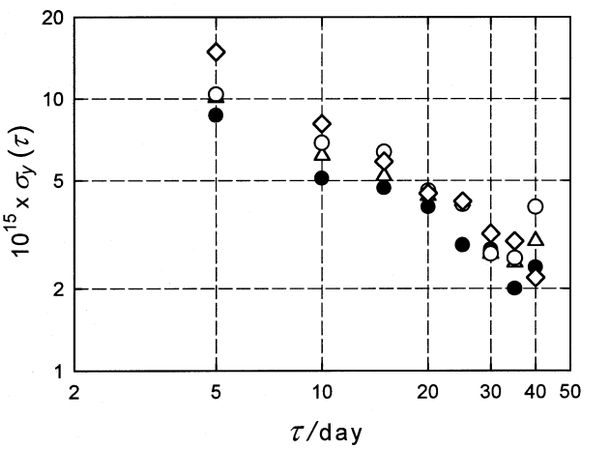

Figure 21. Relative frequency instability of the CS1 determined from comparisons with TAI (●), TA(NIST) (△), TA(USNO) (○) and TA(SU) (◇). Data were obtained from comparisons $[TA(PTB) - T(CS1)]$ and data published in *Circular T* of the BIPM (T113–T123). Error bars due to the finite number of samples are typically $\pm 0.8 \times 10^{-15}$ for the last data point.

should be absent in the future when δF_{BR} will have been determined more often.

Fairly large changes in rate are commonly seen in comparisons with all reference scales, starting around MJD 50690 and lasting for 10 to 15 days. Such features are absent in the comparisons with the local clocks, shown in Figure 17. It may be assumed that, to some extent, the changes are due to the instability of long-distance GPS time comparisons, which form the basis of all international time comparisons.

The $\sigma_y(\tau)$ diagram (Figure 21) reveals an instability mostly governed by white frequency noise for averaging times of up to 40 days. For $\tau = 40$ d, the evaluated frequency instability compared with TAI and TA(SU) almost reflects the predicted shot-noise performance of the CS1. It may be concluded from this that the reference time scales are indeed subject to a remarkably small frequency instability. Repetition of this study after a much longer operating time of the CS1 should make it possible to discriminate between the good and the best reference time scales.

6. Discussion

By definition, the duration of the TAI scale unit should be as close as possible to the SI second on the rotating geoid. This will ensure that TAI is a coordinate time scale which may serve as the ultimate reference time scale in scientific applications. The realization of TAI is based on the data of a large ensemble of commercial caesium clocks and hydrogen masers, and on the data from a small number of accurate primary frequency standards which are referred to in Figure 18. Only these few measurements ensure the accuracy of TAI. The role of the PTB's former CS1 clock was noted

in the Introduction; the role of the new CS1 remains to be judged.

Three years have passed from the interruption of the continuous operation of the old CS1 to the writing of this paper; during this time an uncertainty evaluation of the new CS1 has been given and first results of the clock operation have been presented. The individual contributions to the uncertainty, detailed in Section 4, are considerably reduced compared with the former situation. Have all the contributions been stated correctly? No doubt, the weakest point at the moment is the estimation of the correction for the frequency shift due to the end-to-end phase difference of the cavity. In the near future, a copy of the CS1 microwave cavity will be installed inside the PTB's experimental device CSX, and the distributed phase difference and the temperature sensitivity of this type of microwave cavity will be studied. It is hoped that the outcome of these investigations will allow an improved estimate of the uncertainty contribution.

Have any uncertainty contributions been left unstated? This can be answered only, if at all, by mutual comparisons between primary clocks, preferably those designed and operated by different teams. At present, the performance of the three PTB primary clocks leads us to suspect that there is still some effect unaccounted for. This suspicion is supported by occasional frequency steps which are larger than the individual contributions to the uncertainty budget, and also by the systematic difference between the CS3 and the CS1 of the PTB. The authors have always resisted masking this evident problem either by increasing the uncertainty figures or by stopping operation of the clock furnishing the unwanted results.

References

1. Bauch A., Heindorff T., Schröder R., Fischer B., accepted by *IEEE Trans. Instrum. Meas.*, CPEM98 special issue.
2. Dorenwendt K., *Metrologia*, 1986, **22**, 186-189.
3. Becker G., Fischer B., Kramer G., Müller E. K., *PTB-Mitt.*, 1969, **79**, 77-80.
4. Becker G., *Proc. 2nd Symp. Frequency Standards and Metrology*, 1976; *IEEE Trans. Instrum. Meas.*, 1976, **IM-25**, 458-465.
5. Becker G., *IEEE Trans. Instrum. Meas.*, 1978, **IM-27**, 319-325.
6. Vanier J., Audoin C., *The Quantum Physics of Atomic Frequency Standards*, Bristol and Philadelphia, Adam Hilger, 1989.
7. Müller E. K., unpublished paper, 1973.
8. Bauch A., Heindorff T., Schröder R., Fischer B., *Metrologia*, 1996, **33**, 249-259.
9. Augustin R., Bauch A., Schröder R., *Proc. 11th European Frequency and Time Forum*, 1994, 47-52.
10. De Marchi A., Shirley J., Glaze D. J., Drullinger R., *IEEE Trans. Instrum. Meas.*, **37**, 1988, 185-190.
11. de Boer H., Fischer B., Heindorff T., Schröder R., *Proc. 4th European Frequency and Time Forum*, 1990, 523-526.
12. De Marchi A., Francescangeli O., Bava G.P., *IEEE Trans. Instrum. Meas.*, 1993, **42**, 434-438.
13. Giordano V., Pichon L., Cérez P., Théobald G., *J. Appl. Phys.*, 1995, **78**, 1-8.
14. Schröder R., *Proc. 5th European Frequency and Time Forum*, 1991, 194-200.
15. De Marchi A., *Proc. 5th Russian Symposium "Metrology of Time and Space"*, 1995, 102-109.
16. Itano W. M., Lewis L. L., Wineland D. J., *Phys. Rev. A*, 1982, **25**, 1233-1235.
17. Bauch A., Schröder R., *Phys. Rev. Lett.*, 1997, **78**, 622-625.
18. Simon E., Laurent P., Clairon A., *Phys. Rev. A*, 1998, **57**, 436-439.
19. Guinot B., *Metrologia*, 1997, **34**, 261-290.
20. Thomann P., *Proc. 22nd Annual Precise Time and Time Interval (PTTI) Applications and Planning Meeting*, 1991, NASA Conf. Publ. 3116, 331-335.
21. Bauch A., Heindorff T., *Proc. 8th European Frequency and Time Forum*, 1994, 503-512.
22. Ramsey N. F., *Molecular Beams*, London/New York, Oxford University Press, 1956,
23. Makdissi A., de Clercq E., *Proc. 11th European Frequency and Time Forum*, 1997, 601-604.
24. Shirley J. H., *Proc. 43rd IEEE Annual Frequency Control Symposium*, 1989, 162-167; *IEEE Trans. Instrum. Meas.*, 1997, **46**, 117-121.
25. Cutler L. S., Flory C. A., Giffard R. P., De Marchi A., *J. Appl. Phys.*, 1991, **69**, 2780-2792.
26. Bauch A., Schröder R., *Annalen der Physik*, 1993, **2**, 421-449.
27. De Marchi A., Rovera G. D., Premoli A., *Metrologia*, 1984, **20**, 37-47.
28. Boussert B., Théobald G., Dimarcq N., *Proc. 9th European Frequency and Time Forum*, 1995, 394-396.
29. Bauch A., Heindorff T., Schröder R., *IEEE Trans. Instrum. Meas.*, 1985, **IM-34**, 136-138.
30. Shirley J. H., Lee W. D., Rovera G. D., Drullinger R. E., *IEEE Trans. Instrum. Meas.*, 1995, **44**, 136-139.
31. Audoin C., Jardino M., Cutler L. S., Lacey R. F. C., *IEEE Trans. Instrum. Meas.*, 1978, **IM-27**, 325-329.
32. Thomas C., Weighting factors attributed to measurements of primary frequency standards in estimating the accuracy of TAI, *BIPM Rapport BIPM/98-2*, Sèvres, Bureau International des Poids et Mesures, 1998.
33. Parker T. E., Levine J., *IEEE Trans. Ultras. Ferroel. Frequ. Contr.*, 1997, **44**, 1239-1244.

Received on 22 June 1998 and in revised form on 5 October 1998.